






## Evolution of LISA Observables for Binary Black Holes Lensed by an SMBH

JAKE POSTIGLIONE <sup>1,2</sup> K. E. SAAVIK FORD <sup>1,3,2,4</sup> HENRY BEST <sup>1,2,5</sup> BARRY MCKERNAN <sup>1,3,2,4</sup> AND  
MATTHEW O'DOWD <sup>1,2,5</sup>

<sup>1</sup>*Department of Astrophysics, American Museum of Natural History, New York, NY 10024, USA*

<sup>2</sup>*Graduate Center, City University of New York, 365 5th Avenue, New York, NY 10016, USA*

<sup>3</sup>*Center for Computational Astrophysics, Flatiron Institute, New York, NY 10010, USA*

<sup>4</sup>*Department of Science, BMCC, City University of New York, New York, NY 10007, USA*

<sup>5</sup>*Department of Physics and Astronomy, Lehman College of the CUNY, Bronx, NY 10468, USA*

### ABSTRACT

Binary black holes (BBH) are expected to form and merge in active galactic nuclei (AGN), deep in the potential well of a supermassive black hole (SMBH), from populations that exist in a nuclear star cluster (NSC). Here we investigate the gravitational wave (GW) signature of a BBH lensed by a nearby SMBH. For a fiducial GW150914-like BBH orbiting close to a  $10^8 M_\odot$  SMBH located at  $z = 0.1$ , the lensed GW signal varies in a predictable manner in and out of the LISA detectability band and across frequencies. The occurrence of such signatures has the potential to confound LISA global fit models if they are not modelled. Detection of these sources provide an independent measure of AGN inclination angles, along with detecting warping of the inner disk, and measuring the SMBH spin.

*Keywords:* Active galactic nuclei (16), Black holes (162), Gravitational lensing (670), Gravitational waves (678), Star clusters (1567), Stellar mass black holes (1611)

### 1. INTRODUCTION

The Laser Interferometer Space Antenna (LISA) is a European Space Agency (ESA) flagship mission to observe gravitational waves (GW) in the  $f_{\text{GW}} \sim 0.1 - 100$  mHz frequency range (Amaro-Seoane et al. 2017, 2023), with an expected launch date in the mid-2030s. The mission will consist of 3 satellites forming a single triangular antenna. As a result, LISA will function as something of an ‘omni-scope’ with all simultaneously detected GW convolved together, thus requiring sophisticated data analysis techniques to extract and distinguish signals from various astrophysical sources to create a catalog which can be used by electromagnetic (EM) observers (e.g. Littenberg et al. 2013; Korol et al. 2017; Sberna et al. 2021). The challenging task of de-convolving these overlapping signals can be eased by making some assumptions about the nature of the observed astrophysical sources and their expected associated waveforms (Amaro-Seoane et al. 2023).

Many GW sources are expected to emit in the LISA frequency range, including massive black hole binaries (MBHB—spanning total mass  $\sim 10^{4-7} M_\odot$  (Sesana et al. 2011; Garg et al. 2024), white dwarf binaries (WDB) (Breivik et al. 2018; Littenberg et al. 2020), EMRIs & IMRIs (Kocsis et al. 2011; Amaro-Seoane 2018; Derdzinski et al. 2021; Peng & Chen 2023), and of most importance to this work, stellar origin binary black holes (BBH) in the early stages of their inspiral (Sesana 2016a). These BBH are the same sources that are now routinely detected by higher frequency ground-based GW detectors (currently by the LIGO-Virgo-KAGRA [LVK] Consortium, e.g. (Abbott et al. 2023)). Ground-based GW detectors detect the final inspiral of such BBH, and with a lower strain sensitivity at higher GW frequencies, can detect many systems that LISA cannot observe. However, a number of higher mass, nearby, BBH systems should appear in the LISA band years to decades prior to their detection by ground-based GW observers (e.g. Sesana 2016a; Wagg et al. 2022c; Sberna et al. 2022; McKernan et al. 2024). Such potential multi-band sources open up a wide range of interesting astrophysical questions, which could be answered using coordinated observing campaigns.

The detectability of these BBH systems at wider separations in LISA rests on a number of assumptions: (1)  $a_{b,0}$ , the semi-major axis of the binary at formation (if formed dynamically at smaller semi-major axis than appropriate to the LISA frequency range), (2)  $\dot{a}_b$ , the speed of the semi-major axis decay (if purely GW driven or sped up through gas or dynamical interactions, e.g.  $\ddot{a}_b$ ), (3)  $(a_b, e_b, i_b)$ , the orbital parameters of the system appropriate to the LISA frequency band, including eccentricity around center of mass and inclination of orbit w.r.t. the observer's sight-line, (4)  $dN_b/dt$ , the rate of occurrence BBH (which is related to both their detection rate by ground-based detectors but also the factors listed above).

Many authors have considered the LISA observability of BBH which may form from dynamical channels, notably in globular clusters (e.g. Kremer et al. 2018; Samsing & D’Orazio 2018) or in Active Galactic Nucleus (AGN) accretion disks (e.g. McKernan et al. 2014; Toubiana et al. 2021; Sberna et al. 2022), as well as in isolated binary systems (e.g. Wagg et al. 2022c; van Zeist et al. 2023). The AGN channel of course rests on the assumption of a pre-existing nuclear star cluster (NSC) (e.g. Neumayer et al. 2020). The original GW detection of a BBH, GW150914 (Abbott et al. 2016) is often used as an example case, both because we know such systems exist, and if the system was evolving in vacuum, it *would* have been detectable by LISA (had LISA been observing)  $\sim$  a decade before its merger could be seen from the ground (Sesana 2016a). GW150914-like BBH orbiting close enough to a supermassive black hole (SMBH) in an AGN that we would expect to see strong gravitational lensing effects imprinted on the LISA-observed waveform of the binary are only infrequently considered (e.g. Tamanini et al. 2020; Chen 2021; Kuntz & Leyde 2023; Zwick et al. 2023). While less likely, it is also possible for such a system to form in a gas-poor NSC, where it could experience similar lensing effects.

Gravitational lensing occurs when an object of sufficient mass comes between a GW source and an observer. The lens magnifies the emitted signal, increasing the apparent luminosity of the source. This effect is observed in EM, but should also occur in GW. For LVK mergers, this lensing would cause the binary to appear as high-mass and at a small redshift, but current observations have not confirmed such an event (Chen 2021).

Here we consider the simple case of a BBH orbiting the SMBH on a small, circular, co-planar orbit at 2 different radii within an AGN disk. We further assume the BBH itself has an eccentricity of zero ( $e_b = 0$ ) around its own center of mass. We ignore gas or tidal effects on the BBH evolution, simply assuming vacuum evolution of  $a_b$ ,

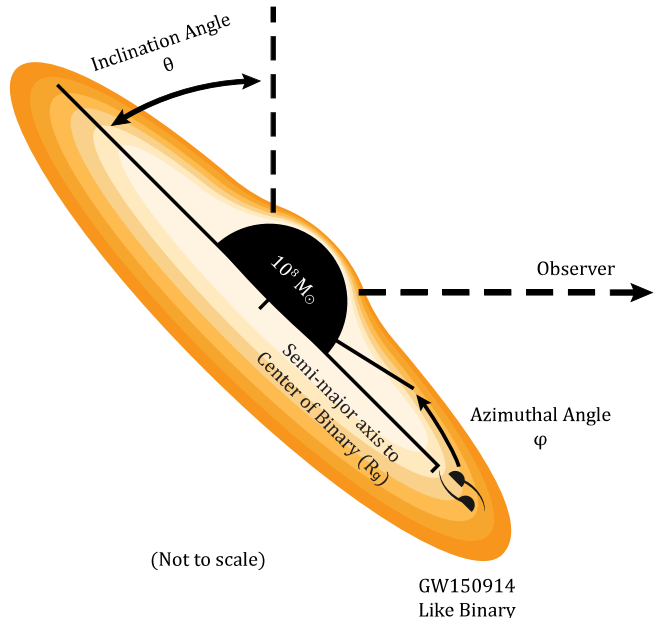


**Figure 1.** Illustration showing the physical setup for the environment in which we consider a GW150914 like binary to be in orbit around a  $10^8 M_{\odot}$  SMBH. The center of mass of the binary is tracked in polar coordinates. The semi-major axis of the binary’s orbit is measured in gravitational radii  $R_g$ . The azimuthal angle  $\varphi$  of the binary in the disk is measured from the axis extending to the observer. The inclination  $\theta$  of the disk is measured from being face on to the observer, with the top of the disk moving away from the observer as the inclination increases.

to examine the impact of lensing on the LISA-observed  $f_{\text{GW}}$  and strain ( $h$ ) from such a source. We invoke AGN channel models for the formation of this hypothetical binary, finding that there is a potential to form a binary very close to the SMBH if multiple single black holes are efficiently delivered to the inner disk (e.g. Secunda et al. 2021). (Bellovary et al. 2016; Peng & Chen 2021) have also shown that migration traps may exist at small disk radii, depending on the model (e.g. Sirko & Goodman 2003), although see also (Grishin et al. 2024). For disks close to edge-on to the observer, BBH at small radii can experience extremely strong gravitational lensing effects from the SMBH, along with strong red-shifting due to the deep gravitational potential. The observed GW waveforms should depart substantially from vacuum expectation and will show strongly perturbed observed strain and frequencies, which will vary with the phase of the BBH orbit around the SMBH (Kuntz & Leyde 2023). The BBH orbital timescale around the SMBH will be much smaller than the LISA mission lifetime, so these signatures varying periodically in  $(f_{\text{GW}}, h)$  must be accounted for if such a source is to be identified in the LISA data stream.

## 2. METHODS

We consider a binary system of the same description as GW150914 with masses of  $36 M_\odot$  and  $29 M_\odot$  placed at a distance of 410 Mpc from a theoretical observer (Abbott et al. 2016). This system was chosen due to having an orbital frequency of  $f_{orb} = 0.8 \times 10^{-3}$  Hz roughly five years before LIGO detected its coalescence, and would have been detectable by LISA had it been observing (Sesana 2016b). We consider this binary in a circular, co-planer orbit, without perturbation, around an SMBH. The mass of the SMBH was chosen to be  $10^8 M_\odot$  to artificially limit the effects of tidal disruption on the binary, if a full numerical simulation was run (see below).

Figure 1 shows the physical setup of our model and how the system is oriented with respect to the observer. We assume the binary to be in a circularized orbit, so the position of the binary’s center of mass is tracked in polar coordinates. The orbital radius  $r$  around the SMBH is measured in units of gravitational radii  $R_g = GM_{\text{SMBH}}/c^2$ . The azimuthal angle is given as  $\varphi$ , where an observer exists along the axis extending from  $\varphi = 0^\circ$ . The inclination angle of the disk  $\theta$  is defined such that a disk with an inclination of  $\theta = 0^\circ$  would be face on to the observer. We can also specify the semi-major axis of the (presumed quasi-circular) BBH as  $a$  (not pictured), as it evolves over time. Throughout the work, we assume an initial semi-major axis of  $a = 1 \times 10^{-3}$  AU, which corresponds to an GW emission frequency of  $f_{obs} = 1.6 \times 10^{-3}$  Hz.

Due to the extremely small values of  $r$  we consider in this work, it is worth checking that our proposed binary is stable to tidal forces from the SMBH. If we compute the value of the Hill Radius,  $R_{\text{Hill}} = r(q/3)^{1/3}$ , where  $q$  is the small mass ratio between the binary and the SMBH, for  $r = 20 R_g$ , we find  $R_{\text{Hill}} > a$ ; were we to substitute a smaller SMBH mass of  $10^6 M_\odot$  (where our proposed binary might also provide a very interesting LISA-detectable EMRI signal) we would unfortunately have  $a > R_{\text{Hill}}$ . Thus, despite the possibly interesting nature of such a source, modeling it would require a more sophisticated approach and is beyond the scope of this work.

### 2.1. Ray tracing

The gravitational potential surrounding a central SMBH is typically described using either the Schwarzschild or the Kerr metric. Assuming that gravitational waves will propagate like photons through this metric (e.g. along null geodesics), we make use of preex-

isting ray-tracing solutions. In particular, we use `Sim5`<sup>1</sup> (Bursa 2017) to trace geodesics from the observer to the mid-plane of an thin inclined accretion disk in the Kerr metric where the spin of the SMBH is set to 0.

Certain regimes of parameter space require proper treatment of gravitational wave propagation using wave optics (D’Orazio & Loeb 2020; Dalang et al. 2022). There are 3 major sources of interference which we should consider: scattering, magnification, and the modulation of the wave’s polarization. In the context of scattering, this may be defined as a three-body system (Pijenburg et al. 2024). Wave optics become important in this type of system when the wavelength of the emitted GWs is longer than the Schwarzschild radius of the SMBH, which is the case when  $f_{\text{GW}} \geq 0.08 \text{ Hz} (10^5 M_\odot / M_{\text{BH}})$  (D’Orazio & Loeb 2020). In this case, at any point of the orbit the GWs may be reflected off the SMBH and scattered to the observer, causing interference with the original waves (Dolan 2008). For  $f_{\text{GW}} = 1.6 \times 10^{-3} \text{ Hz}$ , this corresponds to SMBH with  $M_{\text{BH}} \leq 10^6 M_\odot$ , and our experiment is safely outside this range.

Wave optics may also start becoming important in the context of gravitational lensing of the BBH system. The first order correction to geometric optics tells us that the GW’s tensorial distortion tensor from a lensing event is (Dalang et al. 2022):

$$F_{\mu\nu\alpha\beta} = \left[ m_\mu m_\nu - i \frac{4\Omega R_s}{b^2} e^{2i\beta} n_\mu n_\nu \right] l_\alpha l_\beta + \left[ l_\mu l_\nu - i \frac{4\Omega R_s}{b^2} e^{-2i\beta} n_\mu n_\nu \right] m_\alpha m_\beta \quad (1)$$

with  $\Omega \equiv 2\pi/\lambda$ , and note that this is a first-order approximation for a point-like lens. The first set of terms in the brackets represent the undistorted tensor where geometric optics hold. The second term in each set of brackets represents deviations from the geometric optics regime, which scales  $\propto R_s \lambda^{-1} b^{-2}$  with the SMBH’s Schwarzschild radius, the inverse of the GW’s wavelength, and the inverse square of the impact parameter in gravitational radii. Within our experiment, the configuration most likely to lay outside the geometric optics regime is the inclined accretion disk at  $88^\circ$  with the BBH orbiting the SMBH at  $20 R_g$ . In this orbit when the BBH is farthest from the observer, the impact parameter becomes  $b = 20 \cos 88^\circ \sim 0.7$  (the impact parameter does not depend on the curvature of the metric). The redshifting of the GW by the SMBH’s gravitational well should be considered, which

<sup>1</sup> <https://github.com/mbursa/sim5/>

is approximately 0.5. We consider this by approximating the wavelengths observed by LISA as  $\lambda_{\text{emit}} = \lambda_{\text{obs}}(1+z)^{-1} = cf_{\text{obs}}^{-1}(1+z)^{-1} \approx 10^{-11}\text{m}$ . The distortion of the GW's tensor is on the scale of  $2\pi R_s \lambda_{\text{emit}}^{-1} b^{-2} \approx (10^{11}\text{m})(10^{-11}\text{m}^{-1})(2) \approx 2 \approx b^{-2}$ , meaning this is in the wave optics regime. This is an evolving system so we should determine the fraction of time we are within the wave optics regime. This may be approximated as the arc length of the orbit around the SMBH where the GW's tensor is strongly affected by lensing. This may be estimated as when the correction terms in Eqn. (1) approach a considerable fraction of unity. We take this to be 0.1, defined as BBH positions with impact parameter  $b < \sqrt{10}$  (only those positions behind the SMBH will experience lensing). For an orbit with radius  $R_{\text{orbit}}$  in units of gravitational radii, this is only a region within  $\approx 9^\circ = \arccos\left(\sqrt{(1 - 10/R_{\text{orbit}}^2)/\sin^2(\theta)}\right)$  behind the SMBH. This limit is never reached in the configurations with  $\theta = 65^\circ$  or  $R_{\text{orbit}} = 100R_g$ , and accounts for only  $\sim 5\%$  of the orbit in the configuration  $\theta = 88^\circ, R_{\text{orbit}} = 20R_g$ . Therefore, for our purposes of order of magnitude estimations across the 4 years of observations, we may use geometric optics to approximate the redshifting and amplification due to gravitational lensing.

Wave optics may also be required to determine the change of the GW's polarization. The typical plus and cross polarizations have the ability to interfere with each other if they remain in phase, become circularly polarized if one path around the strong lens accrues a half wavelength phase shift, or a combination of the previous (Pijenburg et al. 2024). This is most important in unresolved multiply imaged systems such as traditional strong lensed systems (see Courbin et al. 2002, for a review on lensing). However, the creation of multiple discrete images requires crossing a *caustic* in the source plane, a region where the magnification formally diverges and leads to the creation or destruction of images. A caustic cannot be produced by a single SMBH, and requires some external shear or imperfect lensing potential. Therefore, we do not consider these effects, as we only are looking at the order of magnitude amplification of the BBH's signal as it orbits around an SMBH. We note that this may be an important consideration in cosmological scale lenses where a galaxy's imperfect Fermat potential leads to the splitting of images.

The projection we use simulates how the accretion disk might appear to an observer after considering light bending effects, if we were able to resolve the  $\sim$ nanoarcsecond angular structure.

Our geodesics define test locations on the accretion disk where the generalized Doppler factor  $g \equiv f_{\text{obs}}/f_{\text{emit}} = 1/(z+1)$  and spatial positioning, important for the calculation of magnification, are recorded. The generalized Doppler factor from this simulation is a sum of both the velocity and gravitationally dependent redshifting a photon emitted from the disk will exhibit.

By considering the positioning of geodesics in the accretion disk and the energy shift of its radiation, we can predict the observed frequency and magnification as functions of time for an evolving binary emitting gravitational waves that are orbiting in the mid-plane.

We set up our ray-tracing simulation by placing the SMBH at the center of the screen and preparing a grid of geodesics which connect the observer to the plane of the accretion disk. This grid extends out  $200 R_g \equiv GM_{\text{SMBH}}/c^2$  in each direction, leading to a 400 by 400  $R_g$  square.

In the case of inclined disks, positive y-values represent looking ‘‘over’’ the SMBH at the far side of the disk. This region of the accretion disk typically appears magnified due to gravitational lensing. It is important to note that, due to light bending effects, the incident shape of the grid onto the inclined disk strays from the its original square-like configuration.

The radial position  $r_{\text{emit}}$ , the azimuthal angle  $\phi_{\text{emit}}$ , and the generalized Doppler factor  $g(r_{\text{emit}}, \phi_{\text{emit}})$  for where a geodesic crosses the mid-plane, correspond to the geodesic's originating point in the grid.

## 2.2. Redshift and Magnification Interpolation

Due to the grid-like structure of the data given by our simulation, it is necessary to interpolate along the orbital path for the redshift and magnification. We utilize the `griddata` function from *SciPy* to interpolate over the data using test points along an orbit with a radius

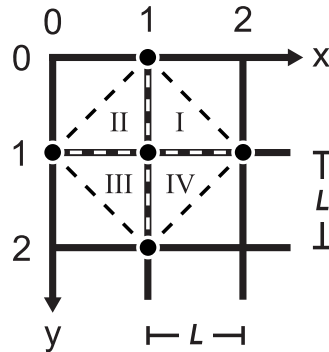


**Figure 2.** Showing the extents of the triangles used to calculate the average magnification for a point at (1, 1). The grid corresponds with the starting position of each geodesics indexed by  $x$  and  $y$ , separated by length  $L$ .



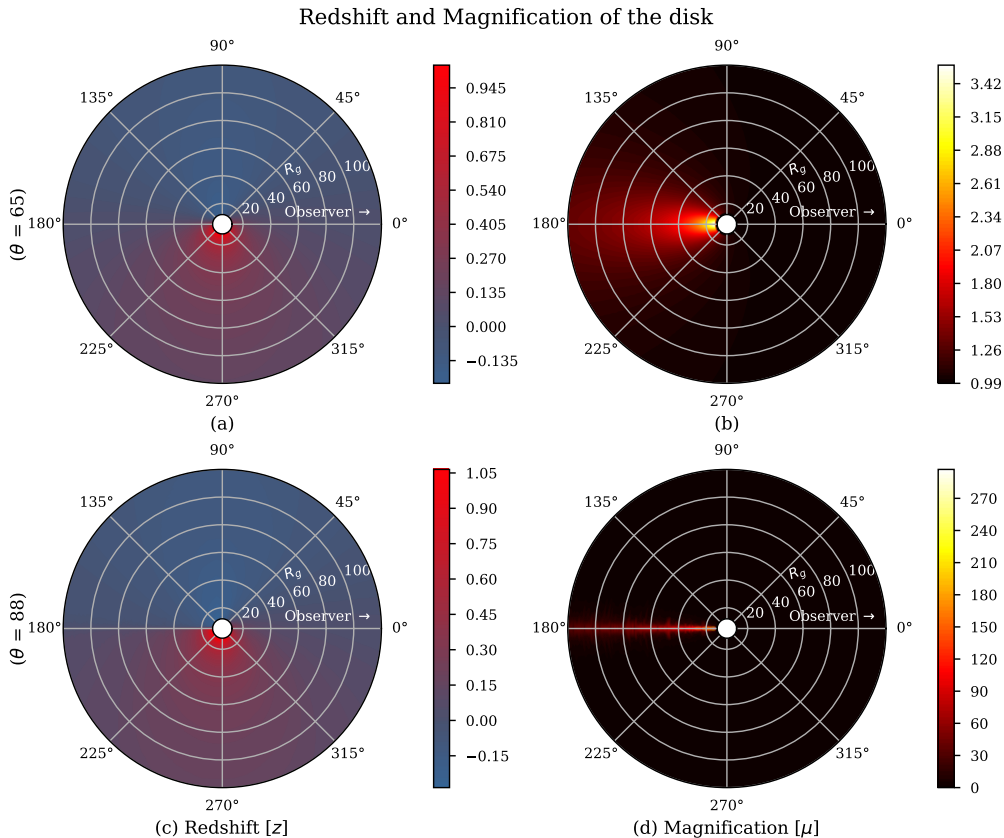


**Figure 3.** Contour plots showing the redshift and magnification sampled across the disk ranging from  $12R_g$  to  $120R_g$  for two separate inclination angles of  $65^\circ$  and  $88^\circ$ . The observer is looking at the disk from an azimuthal angle of  $\theta = 0^\circ$  and the inclination angle is defined such that the  $\varphi = 0^\circ$  case is face on. At higher inclination angles, the top of the disk tilts away relative to the observer’s perspective. Note the difference in scales between the  $65^\circ$  and  $88^\circ$  cases for both redshift and magnification.

defined by  $n$  gravitational radii. As discussed above, redshift is calculated by the simulation, but magnification requires we compare the position of the starting and ending positions of the geodesics. We define this magnification factor as  $\mu = A_{\text{obs}} / (A_{\text{disk}} \cdot \cos\theta_i)$  where  $A_{\text{obs}}$  is the initial area of a triangle formed by three neighboring origin points of geodesics in the grid, and  $A_{\text{disk}}$  is the area of a triangle formed by the same geodesics but instead using the disk-crossing position. Figure 2 shows how the initial triangles are defined using the grid position of geodesics as they are aligned with an integer coordinate grid. The average of four triangles, each respective to a quadrant around an integer coordinate, is used to find the final magnification factor  $\mu$  for one a geodesic. There exist edge cases at the beginning and end of a column or row, where less than four triangles are used to find the average magnification; however, the edges of the grid fall outside of the area we use in our experiment.

We display the resulting maps, zoomed in to range from 12 to  $120 R_g$ , in Figure 3. Plots (a) and (c) show

the interpolated redshift for an inclined disk at  $\theta = 65$  and  $88$  degrees respectively. Plots (b) and (d) show the interpolated magnification for these respective inclinations. Note the difference in scale between the  $65^\circ$  and  $88^\circ$  cases for both Redshift and Magnification.

We consider the binary at both  $20 R_g$  and  $100 R_g$ , near where migration traps are expected to exist, given favorable disk morphology (Bellovary et al. 2016; Peng & Chen 2021). Figure 4 shows the interpolated values for the redshift and magnification as a function of the azimuthal angle ( $\varphi$ ), note the difference in maxima of the interpolated magnification between the  $65^\circ$  and  $88^\circ$  disks. The interpolation is achieved by first reducing the number of co-linear points in the data and then applying an Akima spline, allowing for the interpolation of values while preserving important features (Akima 1970). It is important to note that the peak of the magnification occurs when the redshift is changing *most* rapidly in time, along with the differing in shape of the data and scale of the vertical axis between the different inclination angles.

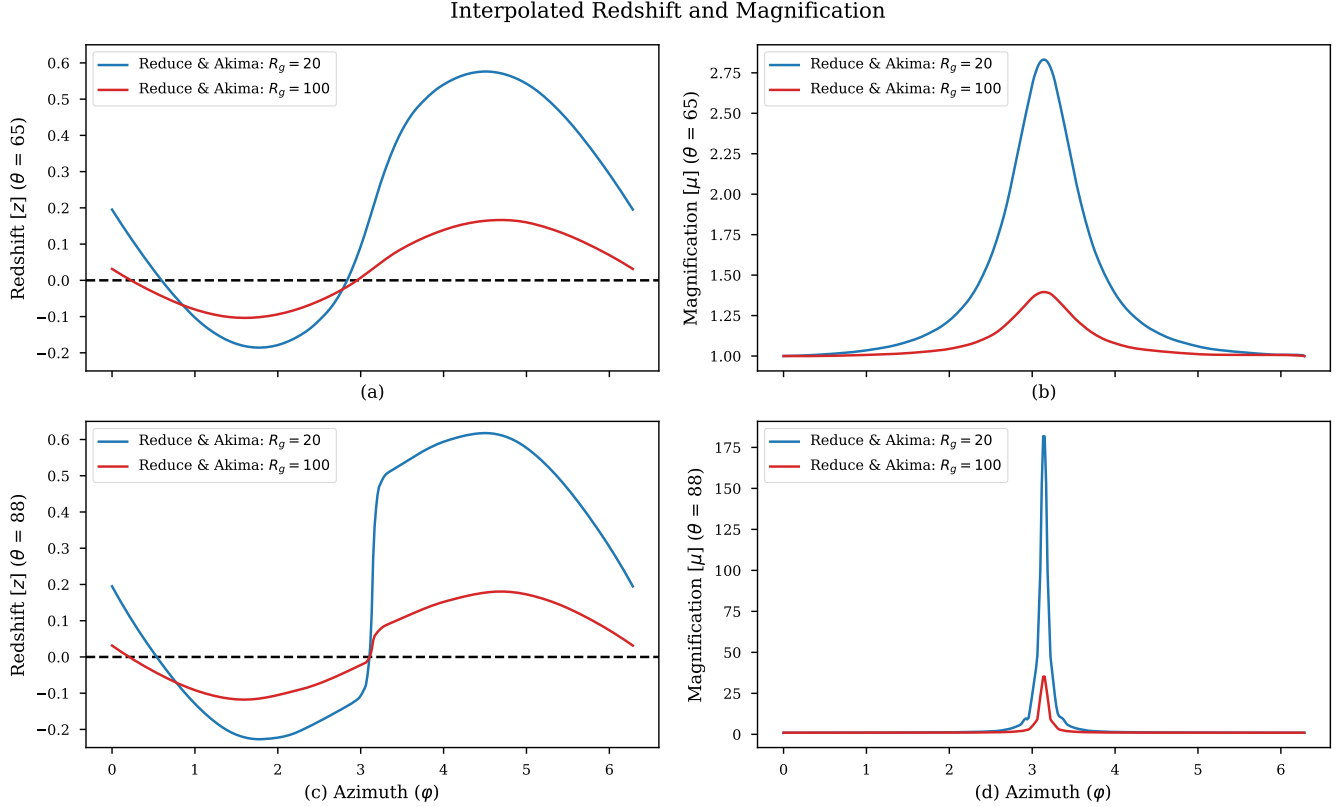


**Figure 4.** Plots showing the interpolated change in redshift and magnification vs azimuthal angle in the disk at gravitational radii of  $20R_g$  and  $100R_g$  for separate inclination angles of  $65^\circ$  and  $88^\circ$ . Note the difference in maxima for the magnification between the two cases.

### 2.3. Binary Evolution

The orbital period  $P$  for a binary orbiting around an SMBH at radius  $r$  in units of  $R_g$  is given by  $P(r) = 2\pi GM_{\text{SMBH}} r^{3/2} c^{-3}$ . The azimuth at which we sample our interpolated redshift and magnification can be found as  $\theta = (2\pi TP^{-1}) \bmod 2\pi$  where  $T$  is the total elapsed time.

We utilize LEGWORK, an open source project developed to predict the evolution of binary sources due to gravitational wave emission (Wagg et al. 2022a,b), producing a baseline for the evolving observed frequency, strain, and characteristic strain. Using the strain amplitude  $h_0$ , as given by LEGWORK for a theoretical observer at a distance of 410 Mpc, we find the magnified strain amplitude as  $h_\mu = h_0 \sqrt{\mu}$  where  $\mu$  is the magnification factor given by the position of the binary along its orbit.

However, this does not account for the fact that the frequency seen by a distant observer is changing rapidly, which changes the *characteristic strain* we would expect to see in the LISA signal, and the inferred SNR for such a source in the LISA data stream. Assuming the system to be circular, isolated, and unperturbed by gas drag or other external dynamical forces, we can

approximate the characteristic strain as  $h_c^2 = \frac{N}{2^{5/3}} h_\mu^2$  where  $N \approx (f_{\text{obs}}^2 / |\dot{f}_{\text{obs}}|)$  over the period of its evolution through the LISA frequency regime.<sup>2</sup>

## 3. RESULTS

Using the interpolated redshift and magnification, shown in Figure 4, to approximate the characteristic strain throughout the evolution of the binary allows us to plot the characteristic strain vs frequency over the LISA sensitivity curve, as seen in Figure 5. The evolution of the isolated binary in a vacuum and assuming pure GR evolution, can be seen in magenta. The first orbit of the binary around the SMBH can be seen in orange, with the entire lifespan of the binary in the LISA frequency range seen in blue.

Since the characteristic strain partially depends on the observed change in gravitational wave frequency, the peaks occurring twice an orbit in Figure 5 do not correlate to the peak in magnification seen in plots (b) and

<sup>2</sup> Since we use the strain amplitude given by LEGWORK, we must account for an extra  $2^{5/3}$  resulting from eq. 17, 26, and 27 in Wagg et al. (2022a,b).

## Approximated Characteristic Strain vs Frequency

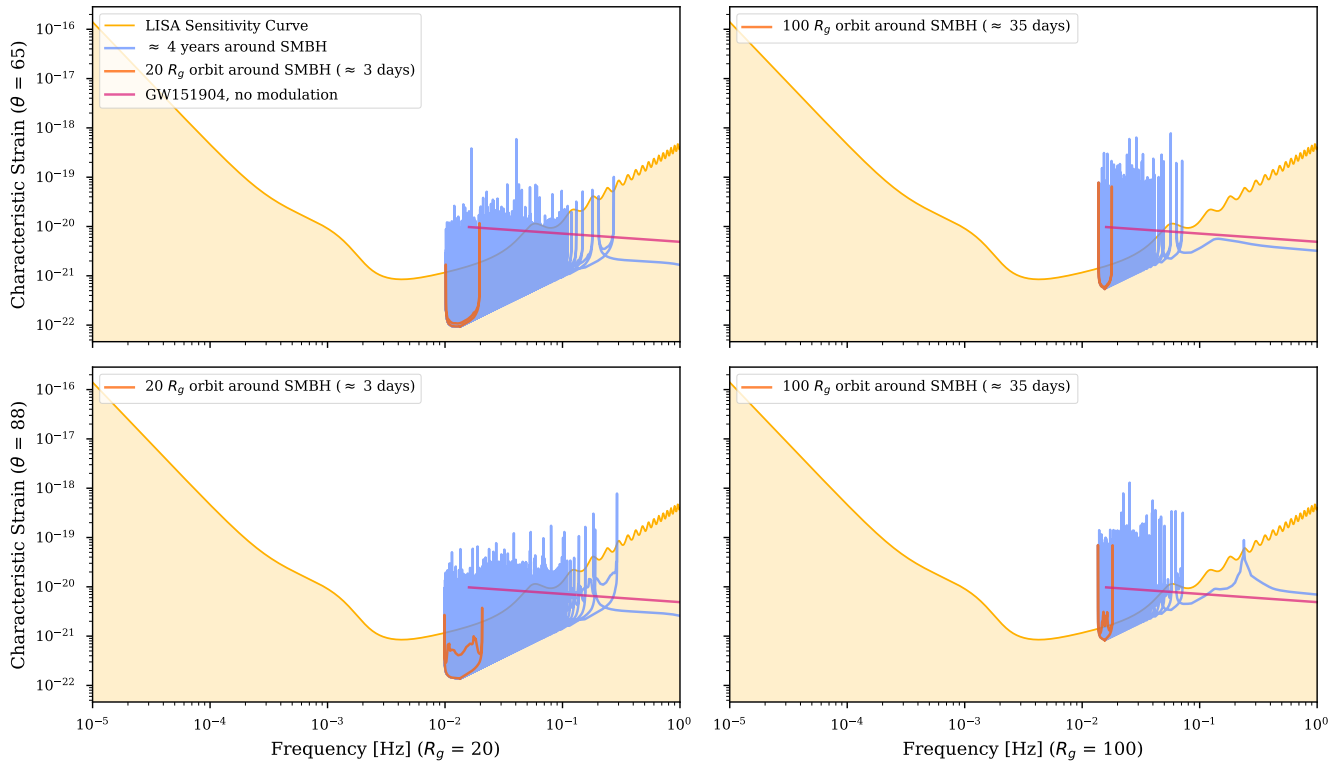


**Figure 5.** Characteristic Strain vs Frequency for a binary at  $20R_g$  and  $100R_g$  in disk with inclinations of  $65^\circ$  and  $88^\circ$ . The two peaks correspond to the where the rate of change of the redshift is small. The minima of the evolution corresponds to when the binary is positioned directly in front of or behind the SMBH, where magnification is at a minimum or maximum, respectively. The  $20R_g$  orbit would have a period of  $\approx 3$  days, with the  $100R_g$  orbit having a period of  $\approx 35$  days. This would correspond to a burst-like signal occurring every 1.5 and 17.5 days respectively.

(d) of Figure 4. When the binary passes behind the SMBH, relative to the sight line of the observer (around an azimuth of  $\varphi \approx \pi$  in Figure 4), the observed strain amplitude is highly magnified. However, the frequency is quickly changing ( $\dot{f}_{\text{obs}}$  is large) due to the rate of change of the redshift. In effect, for both disk inclinations and orbits, the characteristic strain is significantly decreased. In the  $20R_g$  case, this causes the signal to fall below below the LISA sensitivity curve for both inclination angles.

The dual peaks observed in Figure 5, therefore correspond to portions of the orbit where there is *some* magnification and the change in redshift/frequency is slowest ( $\dot{f}_{\text{obs}}$  is near zero). This can be seen around an azimuth of  $\varphi \approx \pi/2$  and  $\varphi \approx 3\pi/2$  in Fig. 4.

We note several additional important trends visible in Fig. 5: going from  $r = 20$  to  $100R_g$  we see the characteristic strains are larger at the same frequencies since the change in  $\dot{f}_{\text{obs}}$  is slower as a result of a larger, slower orbit. Going from an inclination of  $\theta = 65$  to  $88$  degrees, the trace of the plot during an orbit is different since the

magnification factor is higher when the binary is behind the SMBH in the more inclined disk. This feature is present in both  $r = 20$  and  $100R_g$  orbits. Finally, in all cases we note the sharp burst-like quality of the observed lensed signals in the higher frequency region of the LISA band, where background sources are expected to be less common. We will return to this latter point in the discussion section.

## 4. DISCUSSION

## 4.1. Rates and LISA Detectability

In preparation for when LISA starts observing, we want to build a more complete picture of our universe so that we can either confirm the accuracy existing models, or know that new theories need to be developed. To start in this endeavor, we can look at existing rate calculations for the LVK population. The occurrence of BBH mergers near the last migration trap is analytically estimated to be  $\sim 0.4 \text{ Gpc}^{-3} \text{ yr}^{-1}$  for a  $3 \times 10^8 M_\odot$  SMBH in an AGN with a lifespan of  $10^7$  yrs (Peng & Chen 2021). One way to both test and extend this estimate for LISA

would be to utilize a population synthesis code such as *McFACTS* (McKernan et al. 2024). Depending on the properties of the AGN disk used to run *McFACTS*, one would be able to count the occurrence of objects fitting our criteria and assume a rate at which we expect LISA to observe these types of objects.

One thing to consider about the detectability of these types of sources in LISA, is the range or threshold of inclination angles of the disk where we might reasonable expect the change in observed frequency due to Doppler shifting to become larger than width of the frequency bin after some observing times. The width of a frequency bin for LISA is described as the inverse of the total observing time in seconds. For one year, the width of a single bin is expected to be  $\sim 3.169 \times 10^{-8}$  Hz. As such, for LISA to observe an apparent periodic change in frequency, the delta between the extrema of the frequency must be larger than the bin width. Keeping the same assumptions of the system we make earlier, we can approximate the critical inclination angle  $\theta_{\text{crit}}$  at which we would expect the change in frequency to cross into multiple bins:

$$\theta_{\text{crit}} = \arcsin\left(\frac{c}{v_{\text{orb}}}\frac{\alpha - 1}{\alpha + 1}\right) \quad (2)$$

where  $\alpha = \left(\frac{1}{2f_{\text{emit}}T_{\text{obs}}} + 1\right)^2$ ,  $v_{\text{orb}}$  is the orbital velocity,  $f_{\text{emit}}$  is the emitted GW frequency of the black hole binary, and  $T_{\text{obs}}$  is the total observational run time in seconds. For an observational run of 1 year, a binary with a circular orbit at  $20 R_g$ , emitting at a frequency detectable by LISA, would have an detectable frequency shift over multiple bins for disks with inclination angles over  $\sim 4.43 \times 10^{-6}$  rad. Similarly, for a binary at  $100 R_g$ , this would occur in disks with inclination angles over  $\sim 9.90 \times 10^{-6}$  rad. For the  $100 R_g$  case, and assuming a uniform distribution of inclination angles ranging from 0 to  $2\pi$ , only  $\sim 6.3 \times 10^{-4}$  % of disks would have inclinations smaller than the critical angle  $\theta_{\text{crit}}$ .

#### 4.2. A burst, or not a burst, that is the question

Depending on where these sources are in the disk, the observed characteristic strain would spend most of its time below the LISA sensitivity curve (notably and perhaps counterintuitively, this is worse for sources closest to the SMBH, which experience the largest accelerations and therefore suffer from the fastest changing observed frequencies). This may lead to their appearance as “bursty” sources, similar to those expected from Knee et al. (2024). However, unlike the bursts defined in Knee et al. (2024), these sources may be made more detectable by summing the repeated strain contributions

to a particular frequency bin, though the intrinsic evolution of the binary will counteract this. We also note that the “bursts” we expect from this type of source occur at relatively high frequencies within the LISA band, meaning there should be fewer alternative astrophysical sources at the relevant frequencies and strains (Colpi et al. 2024). In principle (as seen in Fig. 5, the sources *are* detectable at their peak characteristic strains, so the problem becomes not one of simple detection, but one of distinguishability—i.e. can we recognize the source of the signal as a real astrophysical source, and determine the astrophysical origin of the signals we observe. The strategies proposed by Knee et al. (2024) should help with this problem.

#### 4.3. Intrinsic Properties of the Disk

Detecting a binary as we described, in an AGN disk, could provide an extremely useful probe of the underlying disk morphology. In our simplified case, it is apparent that one would be able to infer the inclination of the disk (at the orbit of the binary) based on the change in strain amplitude between the binary passing in front of and behind the SMBH. A larger  $\Delta$ strain would be produced by a more edge-on orientation (as is apparent by comparing the lower panels to the upper panels in Fig. 5. On the other hand, a precisely face-on orientation would produce no magnification or time-varying Doppler shift (though there would still be a constant frequency offset from the emitted to observed frequency, due to gravitational redshifting). If the binary is sufficiently close to the SMBH, we would expect the emitted gravitational waves incur effects from relativistic beaming. In such a case, we would expect to see a difference between the local maxima of the two peaks of the characteristic strain, therefore one could determine the phase alignment between the GW observables and other possible observables of the system.

- 1 Support was provided by Schmidt Sciences, LLC. for
- 2 JP, HB & MO. KESF & BM are supported by NSF
- 3 AST- 2206096, NSF AST- 1831415 and Simons Founda-
- 4 tion Grant 533845 as well as Simons Foundation sab-
- 5 batical support. The Flatiron Institute is supported
- 6 by the Simons Foundation. KESF wishes to acknowl-
- 7 edge extremely helpful conversations with Xian Chen
- 8 and Laura Sberna at *New Ideas on the Origin of Black*
- 9 *Hole Mergers* at NBIA, in August 2024. HB acknowl-
- 10 edges the support from the Czech Science Foundation
- 11 (GACR) Junior Star grant no. GM24-10599M.

*Software:* Astropy (Astropy Collaboration et al. 2013, 2018, 2022), LEGWORK (Wag9 et al. 2022a,b),



Matplotlib (Hunter 2007), Numpy (Harris et al. 2020), SciPy (Virtanen et al. 2020), SIM5 (Bursa 2017, 2018)

## REFERENCES

- Abbott, B. P., Abbott, R., Abbott, T. D., et al. 2016, *PhRvL*, 116, 061102, doi: [10.1103/PhysRevLett.116.061102](https://doi.org/10.1103/PhysRevLett.116.061102)
- Abbott, B. P., Abbott, R., Abbott, T. D., et al. 2016, *Phys. Rev. Lett.*, 116, 061102, doi: [10.1103/PhysRevLett.116.061102](https://doi.org/10.1103/PhysRevLett.116.061102)
- Abbott, R., Abbott, T. D., Acernese, F., et al. 2023, *Physical Review X*, 13, 011048, doi: [10.1103/PhysRevX.13.011048](https://doi.org/10.1103/PhysRevX.13.011048)
- Akima, H. 1970, *J. ACM*, 17, 589–602, doi: [10.1145/321607.321609](https://doi.org/10.1145/321607.321609)
- Amaro-Seoane, P. 2018, *PhRvD*, 98, 063018, doi: [10.1103/PhysRevD.98.063018](https://doi.org/10.1103/PhysRevD.98.063018)
- Amaro-Seoane, P., Audley, H., Babak, S., et al. 2017, arXiv e-prints, arXiv:1702.00786, doi: [10.48550/arXiv.1702.00786](https://doi.org/10.48550/arXiv.1702.00786)
- Amaro-Seoane, P., Andrews, J., Arca Sedda, M., et al. 2023, *Living Reviews in Relativity*, 26, 2, doi: [10.1007/s41114-022-00041-y](https://doi.org/10.1007/s41114-022-00041-y)
- Astropy Collaboration, Robitaille, T. P., Tollerud, E. J., et al. 2013, *A&A*, 558, A33, doi: [10.1051/0004-6361/201322068](https://doi.org/10.1051/0004-6361/201322068)
- Astropy Collaboration, Price-Whelan, A. M., Sipőcz, B. M., et al. 2018, *AJ*, 156, 123, doi: [10.3847/1538-3881/aabc4f](https://doi.org/10.3847/1538-3881/aabc4f)
- Astropy Collaboration, Price-Whelan, A. M., Lim, P. L., et al. 2022, *ApJ*, 935, 167, doi: [10.3847/1538-4357/ac7c74](https://doi.org/10.3847/1538-4357/ac7c74)
- Bellovary, J. M., Mac Low, M.-M., McKernan, B., & Ford, K. E. S. 2016, *ApJL*, 819, L17, doi: [10.3847/2041-8205/819/2/L17](https://doi.org/10.3847/2041-8205/819/2/L17)
- Breivik, K., Kremer, K., Bueno, M., et al. 2018, *ApJL*, 854, L1, doi: [10.3847/2041-8213/aaa23](https://doi.org/10.3847/2041-8213/aaa23)
- Bursa, M. 2017, in *RAGtime 17-19: Workshops on Black Holes and Neutron Stars*, 7–21
- Bursa, M. 2018, *SIM5: Library for ray-tracing and radiation transport in general relativity*, *Astrophysics Source Code Library*, record ascl:1811.011
- Chen, X. 2021, *Distortion of Gravitational-Wave Signals by Astrophysical Environments*, doi: [10.1007/978-981-15-4702-7\\_39-1](https://doi.org/10.1007/978-981-15-4702-7_39-1)
- Colpi, M., Danzmann, K., Hewitson, M., et al. 2024, *LISA Definition Study Report*. <https://arxiv.org/abs/2402.07571>
- Courbin, F., Saha, P., & Schechter, P. L. 2002, *Quasar Lensing*, Vol. 608, 1
- Dalang, C., Cusin, G., & Lagos, M. 2022, *PhRvD*, 105, 024005, doi: [10.1103/PhysRevD.105.024005](https://doi.org/10.1103/PhysRevD.105.024005)
- Derdzinski, A., D’Orazio, D., Duffell, P., Haiman, Z., & MacFadyen, A. 2021, *MNRAS*, 501, 3540, doi: [10.1093/mnras/staa3976](https://doi.org/10.1093/mnras/staa3976)
- Dolan, S. R. 2008, *Classical and Quantum Gravity*, 25, 235002, doi: [10.1088/0264-9381/25/23/235002](https://doi.org/10.1088/0264-9381/25/23/235002)
- D’Orazio, D. J., & Loeb, A. 2020, *PhRvD*, 101, 083031, doi: [10.1103/PhysRevD.101.083031](https://doi.org/10.1103/PhysRevD.101.083031)
- Garg, M., Sberna, L., Speri, L., Duque, F., & Gair, J. 2024, arXiv e-prints, arXiv:2410.02910, doi: [10.48550/arXiv.2410.02910](https://doi.org/10.48550/arXiv.2410.02910)
- Grishin, E., Gilbaum, S., & Stone, N. C. 2024, *MNRAS*, 530, 2114, doi: [10.1093/mnras/stae828](https://doi.org/10.1093/mnras/stae828)
- Harris, C. R., Millman, K. J., van der Walt, S. J., et al. 2020, *Nature*, 585, 357–362, doi: [10.1038/s41586-020-2649-2](https://doi.org/10.1038/s41586-020-2649-2)
- Hunter, J. D. 2007, *Computing in Science & Engineering*, 9, 90, doi: [10.1109/MCSE.2007.55](https://doi.org/10.1109/MCSE.2007.55)
- Knee, A. M., McIver, J., Naoz, S., et al. 2024, *The Astrophysical Journal Letters*, 971, L38, doi: [10.3847/2041-8213/ad6a10](https://doi.org/10.3847/2041-8213/ad6a10)
- Kocsis, B., Yunes, N., & Loeb, A. 2011, *PhRvD*, 84, 024032, doi: [10.1103/PhysRevD.84.024032](https://doi.org/10.1103/PhysRevD.84.024032)
- Korol, V., Rossi, E. M., Groot, P. J., et al. 2017, *MNRAS*, 470, 1894, doi: [10.1093/mnras/stx1285](https://doi.org/10.1093/mnras/stx1285)
- Kremer, K., Chatterjee, S., Breivik, K., et al. 2018, *PhRvL*, 120, 191103, doi: [10.1103/PhysRevLett.120.191103](https://doi.org/10.1103/PhysRevLett.120.191103)
- Kuntz, A., & Leyde, K. 2023, *PhRvD*, 108, 024002, doi: [10.1103/PhysRevD.108.024002](https://doi.org/10.1103/PhysRevD.108.024002)
- Littenberg, T. B., Cornish, N. J., Lackeos, K., & Robson, T. 2020, *PhRvD*, 101, 123021, doi: [10.1103/PhysRevD.101.123021](https://doi.org/10.1103/PhysRevD.101.123021)
- Littenberg, T. B., Larson, S. L., Nelemans, G., & Cornish, N. J. 2013, *MNRAS*, 429, 2361, doi: [10.1093/mnras/sts507](https://doi.org/10.1093/mnras/sts507)
- McKernan, B., Ford, K. E. S., Cook, H. E., et al. 2024, arXiv e-prints, arXiv:2410.16515, doi: [10.48550/arXiv.2410.16515](https://doi.org/10.48550/arXiv.2410.16515)
- McKernan, B., Ford, K. E. S., Cook, H. E., et al. 2024. <https://arxiv.org/abs/2410.16515>
- McKernan, B., Ford, K. E. S., Kocsis, B., Lyra, W., & Winter, L. M. 2014, *MNRAS*, 441, 900, doi: [10.1093/mnras/stu553](https://doi.org/10.1093/mnras/stu553)

- Neumayer, N., Seth, A., & Böker, T. 2020, *A&A Rv*, 28, 4, doi: [10.1007/s00159-020-00125-0](https://doi.org/10.1007/s00159-020-00125-0)
- Peng, P., & Chen, X. 2021, *MNRAS*, 505, 1324, doi: [10.1093/mnras/stab1419](https://doi.org/10.1093/mnras/stab1419)
- . 2023, *ApJ*, 950, 3, doi: [10.3847/1538-4357/acce3b](https://doi.org/10.3847/1538-4357/acce3b)
- Pijnenburg, M., Cusin, G., Pitrou, C., & Uzan, J.-P. 2024, *PhRvD*, 110, 044054, doi: [10.1103/PhysRevD.110.044054](https://doi.org/10.1103/PhysRevD.110.044054)
- Samsing, J., & D’Orazio, D. J. 2018, *MNRAS*, 481, 5445, doi: [10.1093/mnras/sty2334](https://doi.org/10.1093/mnras/sty2334)
- Sberna, L., Toubiana, A., & Miller, M. C. 2021, *ApJ*, 908, 1, doi: [10.3847/1538-4357/abccc7](https://doi.org/10.3847/1538-4357/abccc7)
- Sberna, L., Babak, S., Marsat, S., et al. 2022, *PhRvD*, 106, 064056, doi: [10.1103/PhysRevD.106.064056](https://doi.org/10.1103/PhysRevD.106.064056)
- Secunda, A., Hernandez, B., Goodman, J., et al. 2021, *ApJL*, 908, L27, doi: [10.3847/2041-8213/abe11d](https://doi.org/10.3847/2041-8213/abe11d)
- Sesana, A. 2016a, *PhRvL*, 116, 231102, doi: [10.1103/PhysRevLett.116.231102](https://doi.org/10.1103/PhysRevLett.116.231102)
- . 2016b, *PhRvL*, 116, 231102, doi: [10.1103/PhysRevLett.116.231102](https://doi.org/10.1103/PhysRevLett.116.231102)
- Sesana, A., Gair, J., Berti, E., & Volonteri, M. 2011, *PhRvD*, 83, 044036, doi: [10.1103/PhysRevD.83.044036](https://doi.org/10.1103/PhysRevD.83.044036)
- Sirko, E., & Goodman, J. 2003, *MNRAS*, 341, 501, doi: [10.1046/j.1365-8711.2003.06431.x](https://doi.org/10.1046/j.1365-8711.2003.06431.x)
- Tamanini, N., Klein, A., Bonvin, C., Barausse, E., & Caprini, C. 2020, *PhRvD*, 101, 063002, doi: [10.1103/PhysRevD.101.063002](https://doi.org/10.1103/PhysRevD.101.063002)
- Toubiana, A., Sberna, L., Caputo, A., et al. 2021, *PhRvL*, 126, 101105, doi: [10.1103/PhysRevLett.126.101105](https://doi.org/10.1103/PhysRevLett.126.101105)
- van Zeist, W. G. J., Eldridge, J. J., & Tang, P. N. 2023, *MNRAS*, 524, 2836, doi: [10.1093/mnras/stad1976](https://doi.org/10.1093/mnras/stad1976)
- Virtanen, P., Gommers, R., Oliphant, T. E., et al. 2020, *Nature Methods*, 17, 261, doi: [10.1038/s41592-019-0686-2](https://doi.org/10.1038/s41592-019-0686-2)
- Wagg, T., Breivik, K., & de Mink, S. 2022a, *The Journal of Open Source Software*, 7, 3998, doi: [10.21105/joss.03998](https://doi.org/10.21105/joss.03998)
- Wagg, T., Breivik, K., & de Mink, S. E. 2022b, *ApJS*, 260, 52, doi: [10.3847/1538-4365/ac5c52](https://doi.org/10.3847/1538-4365/ac5c52)
- Wagg, T., Broekgaarden, F. S., de Mink, S. E., et al. 2022c, *ApJ*, 937, 118, doi: [10.3847/1538-4357/ac8675](https://doi.org/10.3847/1538-4357/ac8675)
- Zwick, L., Capelo, P. R., & Mayer, L. 2023, *MNRAS*, 521, 4645, doi: [10.1093/mnras/stad707](https://doi.org/10.1093/mnras/stad707)